

Angular and Charge State Distributions of Highly Charged Ions Scattered During Low Energy Surface-Channeling Interactions with Au(110)

F.W. Meyer, L. Folkerts, and S. Schippers*

Oak Ridge National Laboratory, Oak Ridge, Tennessee 37831-6372

RECEIVED

SEP 23 1984

OSTI

Abstract

We have measured scattered projectile angular and charge state distributions for 3.75 keV/amu O^{q+} ($3 \leq q \leq 8$) and 1.2 keV/amu Ar^{q+} ($3 \leq q \leq 14$) ions grazing incident along the [110] and [100] directions of a Au(110) single crystal target. Scattered projectile angular distribution characteristic of surface channeling are observed. For both incident species, the dominant scattered charge fraction is neutral, which varies only by a few percent as a function of incident charge state. Significant O^- formation is observed, which manifests a distinct velocity threshold. For incident Ar projectiles with open L-shells, the positive scattered charge fractions, while always less than about 10%, increase linearly with increasing number of initial L-shell vacancies.

Introduction

Most experimental work to date in the area of multicharged ion-surface interactions has focused on measurement of x-ray^{1,2} and electron emission. The latter experiments include measurements of total electron yields, determined either by conventional means³ or via analysis of the electron emission statistics⁴, as well as of ejected electron energy distributions⁵⁻⁷. Recently, H. Winter et al.⁸ directed attention to the scattered projectiles, measuring angular distributions of highly charged ions scattered during grazing surface collisions. They found characteristic shifts of the angular distributions away from the specular reflection angle, which they attributed to image charge acceleration of the highly charged ion during its approach to the surface. The only previous measurement of scattered ion charge state distributions

MASTER

ds

DISTRIBUTION OF THIS DOCUMENT IS UNLIMITED

1

"The submitted manuscript has been authored by a contractor of the U.S. Government under contract DE-AC05-84OR21400. Accordingly, the U.S. Government retains a nonexclusive, royalty-free license to publish or reproduce the published form of this contribution, or allow others to do so, for U.S. Government purposes."

DISCLAIMER

Portions of this document may be illegible in electronic image products. Images are produced from the best available original document.

was made by de Zwart et al.⁹, who measured relative yields of +1, +2, and +3 scattered ions as a function of incident charge state ($q = 1$ to 11) for 20 keV Ne, Ar, and Kr ions incident at 15° on a polycrystalline W target. Since their experiment could not detect neutral scattered projectiles, de Zwart et al. were not able to determine absolute charge state fractions.

In this contribution we describe an experiment in which both the angular as well as charge state distributions of the scattered ions are measured using a two-dimensional position sensitive detector (PSD). The method permits detection of all possible scattered charge states (i.e. including positive ions, neutrals and negative ions), making possible for the first time the extraction of absolute scattered projectile charge fractions. Furthermore, the present measurements were performed under surface channeling conditions as verified by observation of characteristic angular distributions for the reflected projectiles. Under surface channeling conditions there is minimal penetration of the target surface plane and the projectile trajectories are well defined. As a result the interaction times of the projectile with the target can in principle be accurately determined.

Experimental Approach

In the present experiment multicharged O and Ar ions, produced by a CAPRICE ECR ion source at the ORNL Multicharged Ion Research Facility, are grazingly incident ($\Psi = 1.8^\circ$) on a clean Au(110) surface along the [110] or [001] directions. The incident multicharged ion beam is collimated by two 0.5-mm-diameter apertures to an angular divergence of about 0.1° FWHM. The scattering geometry is indicated schematically in Fig. 1. The single crystal Au(110) target is mounted on an x-y-z manipulator located in a UHV chamber having a base pressure of 3×10^{-10} mbar and is prepared by cycles of surface sputter cleaning with 1-keV Ar^+ ions and crystal annealing at about 700°C . Surface cleanliness is verified using electron-induced Auger electron spectroscopy. Both the angular distribution (polar as well as lateral) and charge state distribution of the scattered (reflected) projectiles were measured using a two-dimensional position

sensitive detector (PSD) (Quantar Technology Model 3394A) having a 40-mm-diameter active area. Movable slits located between the target and the PSD were completely opened for measurements of angular scattering distributions. For the charge state distribution measurements they were closed to select a thin vertical slice of the scattered beam, which was then dispersed by charge state across the face of the PSD using a pair of electrostatic deflection plates located immediately downstream of the slit assembly, as shown in Fig. 1. The target-PSD distance is about 560 mm. The PSD is mounted on a second x-y-z manipulator which permits measurement of the polar scattering angle, ϕ_p , in the range -0.8° to $+5.6^\circ$. The position of the primary beam, used to determine $\phi_p=0^\circ$, as well as its angular spread, can thus be directly measured. In order to avoid saturation of the PSD, beam intensities on target were kept sufficiently low that the total scattered ion flux on the PSD did not exceed 100 kHz.

Experimental Results

Figures 2a and 2b show the angular distributions observed on the PSD for two different incident ions and target azimuthal orientations. The characteristic "banana" shape of the angular distributions displayed in the figure is indicative of surface channeling, which occurs whenever the direction of the grazing incident beam is nearly parallel to one of the low index crystal directions, such that the ions are reflected by a series of relatively soft encounters with successive atoms along a particular lattice row rather than a single hard encounter with an isolated lattice atom. The resulting guided motion down the atomic rows leads to an observed angular distribution of the ultimately reflected particles that mirrors the "corrugation" present in the surface. For the [110] direction, this "corrugation" is 8.15 Å wide due to the known (1x2) reconstruction of the Au(110) surface at room temperature, while for the [001] direction, i.e. transverse to the "missing row" direction, it is 4.07 Å. It is noted that the above "banana" shaped angular distribution is no longer observed when the azimuthal crystal orientation is changed a few degrees away from the low-index

directions, or when the crystal is heated above the temperature at which the phase change to the random (1x1) surface reconstruction occurs. It is further noted that already at the above collision energy, the central spot of maximum scattered ion intensity is observed at angles larger than the specular reflection angle, due to image acceleration effects⁸ on the incoming projectile trajectory.

As already mentioned in an earlier section, in order to determine the charge distribution of the scattered ions, movable slits were used to select a vertical slice of the scattered beam, which then passes through a set of deflection plates. The electrostatic analysis produces a series of horizontally displaced vertical bands, each corresponding to a particular charge state, while the intensity distribution of each band along the vertical axis reflects its polar angular distribution. The result of such an electrostatic analysis is shown in Fig. 3 for 3.75 keV/amu O^{8+} ions incident on Au(110) under the same conditions already described in connection with Fig. 2a. The movable slits were set to select lateral angles ϕ_1 from -0.15° to $+0.15^\circ$, i.e. a central slice from the scattered ion angular distribution, while the PSD was shifted horizontally to permit dispersal of the charge state distribution over the full width of the PSD. The vertical bands corresponding to the different charge states are easily discerned in the figure. The band second from the right is the most intense, and corresponds to the neutral component, with negative ions ($r = -1$) on the extreme right and the positive charge states ($r = +1$ to $+5$) to the left. Individual vertical slices (i.e. charge states) can be projected onto the vertical axis, providing information on the polar angular distribution for a particular scattered charge state. This is illustrated in Fig. 4a for four scattered charge states resulting from grazing interactions of O^{8+} with Au(110) along the [110] direction.

Alternatively, charge state distributions can be obtained by essentially collapsing the 2D spectrum onto the horizontal axis, as is illustrated in Fig. 4b. Integration under each charge state "peak" then permits determination of the scattered charge state fractions. This was done for oxygen ions in initial charge states down to $q = 3$, and for Ar ions in the incident charge state range 3-14. The measurement results are given

in Figs. 5 and 6, where the fractions of final charge states "r" are plotted as a function of the incident charge state "q".

Scattered ion charge state distributions were also measured for ion incidence along arbitrary "random" directions, i.e. away from the low-index channels. Only slight variations with incident direction were found in the relative scattered charge fractions. Measurements¹⁰ with incident Ar^{q+} ions, to be discussed in detail elsewhere, showed significant variation of the positive charge fractions as a function of elapsed time since the last annealing cycle, suggesting possible sensitivity of the measured fractions to surface order and/or contamination. It is emphasized, however, that in the present article, the focus is not on the dependences of the charge fractions on target conditions, but rather on their dependence on the incident projectile.

To that end, measurements were also made of the energy dependence of the scattered charge fractions for incident O¹⁺, O⁵⁺ and O⁷⁺ ions in the velocity 0.064 to 0.55 (in a.u.). The positively charged scattered ion fractions show significant increases in the investigated energy range, as might be expected in analogy to gas phase collisions where stripping cross sections steeply increase with energy and the electron capture cross sections are either still flat or have already started to fall. More interestingly, as can be seen in Fig. 7, the fraction of O⁻ ions, which constitute the most loosely bound system ($E_A = 1.48$ eV) in the ensemble of possible charge states, shows a definite velocity or energy "threshold" at $v = 0.1$ a.u., below which the O⁻ fraction is very small, and above which it steadily increases up to the maximum investigated velocity. This velocity dependence is in contrast to what is expected for thick target gas phase collisions¹¹ for this energy interval, where the detachment cross section increases and the σ_{0-1} capture cross is approximately flat or already falling.

Discussion

In order to gain some insight into the trajectories along which the projectiles travel under the conditions of surface-channeling, a Monte Carlo simulation was carried out in which the equations of motion of the projectile in the periodic potential

of the crystal surface were solved for an ensemble of appropriate random initial conditions. Following Niehof and Heiland¹², the scattering potential used was a superposition of individual contributions (assuming a ZBL interaction potential) from a 3x3x3 lattice cell that was progressively translated along the ion trajectory, and that was characterized by a surface Debye temperature of 111 K. Figure 8 shows the simulation results for 3.75 keV/amu O projectiles incident along the [110] direction of Au(110) at 1.8°. As can be seen, quite good agreement with the experimentally measured angular distribution shown in Fig. 2a is obtained. The simulation indicates a total trajectory length within 2 Å of the topmost Au surface layer of about 280 Å, corresponding to an interaction time of only about 30 fs, and a maximum penetration depth of 1.2 Å. This result can be used together with the measured charge distributions to determine time scales¹³ of projectile charge equilibration during multicharged ion-surface interactions.

As regards the charge state distributions for O^{q+} and Ar^{q+} ions shown in Figures 5 and 6, a number of remarkable features can be noted. For all incident charge states investigated, the neutral fraction strongly dominates the scattered ion charge state distribution, as has been already noted by Winter et al.⁸ For incident ions not carrying inner shell vacancies, i.e. $q \leq 6$ for the O ions and $q \leq 8$ for the Ar ions, the scattered charge fractions are essentially independent of incident charge, indicating complete charge equilibration. For the incident oxygen ions, a significant fraction of the scattered ions recede from the surface in charge state -1. As can be seen from Fig. 5, the scattered ion fractions of charge state +2 and higher show noticeable increases when the incident ion carries initial K-shell vacancies, i.e. for O⁷⁺ and O⁸⁺. Such a trend has been previously noted by de Zwart et al.⁹ In the case of the Ar^{q+} incident ions, this increase occurs when the incident ion carries one or more L-shell vacancies, and is evident already in the +1 charge fraction. As is shown in Fig. 6, there is a monotonic increase in all positive charge fractions with increasing initial L-vacancy number, which is seen to become increasingly steeper with increasing scattered charge state. It should be noted, however, that, independent of incident charge state, the overall contribution of scattered charge states +1 and higher to the

total scattered ion intensity is less than 10% for the two systems and energies investigated.

The scattered projectile polar angular distributions shown in Fig. 4a show evidence of two components. The first one, which dominates the low scattered charge state angular distributions, is narrow with FWHM about 1° and peaks close to the angle expected for specular reflection. The second is significantly broader and shifted to smaller scattering angles. The latter component appears to increase in relative importance with increasing charge state, and appears to be the dominant one for scattered charge state +3. It is possible that this broader component results from the small fraction of projectiles in which inner-shell Auger decay takes place on the outgoing trajectory, but the data analysis required to resolve this issue is presently still incomplete.

For the case of the incident oxygen ions, the velocity threshold observed for the scattered O^- fraction (see Fig. 7) can be used¹³ to estimate the spatial extent of charge equilibration on the receding part of the projectile trajectory. Negative ion formation velocity thresholds such as displayed in Fig. 7 can be explained as arising due to "kinematic resonance" effects¹⁴ in the case of projectiles having non-zero parallel velocity components with respect to the target surface. In the rest frame of such projectiles, a modification of the Fermi-Dirac distribution of target electrons results in a virtual population of electronic states above the Fermi edge. At sufficiently high parallel velocities, occupied states of the solid can come into resonance with a projectile negative ion level whose electron affinity is significantly less than the surface work function of the target. This scenario is schematically indicated in the inset of Fig. 7. An additional feature of negative ion formation above metal surfaces is the fact that, unlike ionization energies of positive ions, the negative ion electron affinity increases with decreasing distance to the surface, due to the image charge interaction which shifts the negative ion binding energy by $-1/4z$, where z is the distance above the surface (energy shift and distance in atomic units). This has the consequence that, from the measured threshold of negative ion formation, the maximum distance of negative ion formation above the surface can be inferred. For

the threshold observed in the present case, the top of the kinematically shifted valence electron distribution is within 0.128 a.u. of the vacuum level, implying a negative ion level shift due to the image charge interaction of -0.074 a.u. at that point. This shift corresponds to a distance of formation of $\sim 3a_0$. Under the assumption that the O^- ion is formed by a one electron transfer process, neutral oxygen is a necessary precursor. The fact that both the neutral and O^- fractions are essentially independent of incident charge state indicates that the above noted charge equilibration is already essentially complete while the scattered ions are still within $3 a_0$ of the surface.

To estimate the contribution to charge equilibration of the above-surface resonance neutralization and autoionization cascade occurring on the approach trajectory, simulations for various oxygen charge states incident on Au(110) were carried out using the code developed by Burgdörfer et al.¹⁵ to determine the resulting electron populations in the various projectile n-levels at the time of surface impact. Particularly for the highest oxygen charge states, i.e. +7 and +8, which have the longest autoionization cascades to be traversed in order to populate the inner shells, at the perpendicular velocity corresponding to the experimental condition of Fig. 5, only little feeding of the projectile K-, L-, and M- shells via the autoionization cascade was found. The other captured electrons remain in higher lying Rydberg levels, where they will be peeled from the projectile by the increased screening it will experience upon reaching the surface. It is concluded¹³ that inner shell electron population along the approach trajectory via the above-surface cascade does not play a significant direct role in the charge equilibration of these highly charged ions during their interaction with the surface.

It thus appears that, at least for the incident O^{q+} ions, even for the grazing collisions studied here, the dominant contribution to the charge equilibration comes from the close interaction with the surface, i.e. within roughly $3 a_0$ of the surface.

DISCLAIMER

This report was prepared as an account of work sponsored by an agency of the United States Government. Neither the United States Government nor any agency thereof, nor any of their employees, makes any warranty, express or implied, or assumes any legal liability or responsibility for the accuracy, completeness, or usefulness of any information, apparatus, product, or process disclosed, or represents that its use would not infringe privately owned rights. Reference herein to any specific commercial product, process, or service by trade name, trademark, manufacturer, or otherwise does not necessarily constitute or imply its endorsement, recommendation, or favoring by the United States Government or any agency thereof. The views and opinions of authors expressed herein do not necessarily state or reflect those of the United States Government or any agency thereof.

Acknowledgements

This research was sponsored by the Division of Applied Plasma Physics, Office of Fusion Energy, and by the Division of Chemical Sciences, Office of Basic Energy Sciences of the U.S. Department of Energy under contract No. DE-AC05-84OR21400 with Martin Marietta Energy Systems, Inc. L. Folkerts was supported through a program administered by the Oak Ridge Institute for Science and Education. S. Schippers gratefully acknowledges financial support by the Deutsche Forschungsgemeinschaft (DFG).

References

*Present address: Kerfysisch Versneller Instituut, Zernikelaan 25, 9747 AA Groningen, The Netherlands.

¹B. D'Etat, J.P. Briand, G. Ban, L. de Billy, P. Briand, J.P. Desclaux, G. Melin, T. Lamy, G. Lamboley, P. Richard, M. Stockli, R. Ali, N. Renard, D. Schneider, M. Clark, P. Beiersdorfer, and V. Decaux, HCl 1992 Invited Papers, Manhattan, Kansas.

²H.J. Andrä, A. Simionovici, T. Lamy, A. Brenac, G. Lamboley, A. Pesnelle, S. Andriamonje, A. Fleury, M. Bonnefoy, M. Chassevent, and J.J. Bonnet, ICPEAC XVII Invited Papers, Brisbane, Australia, p. 89, 1991.

³M. Fehring, M. Delaunay, R. Geller, P. Varga, and HP. Winter, NIM B23, 245 (1987).

⁴F. Aumayr and HP. Winter, Comments At. Mol. Phys. 29, 275 (1994).

⁵F.W. Meyer, S.H. Overbury, C.C. Havener, P.A. Zeijlmans van Emmichoven, J. Burgdörfer, and D.M. Zehner, Phys. Rev. A44, 7214 (1991).

⁶R. Köhrbrück, M. Grether, A. Spieler, N. Stolterfoht, R. Page, A. Saal, and J. Bleck-Neuhaus, Phys. Rev. A49, xxxx (1994).

⁷J. Das, H. Limburg, and R. Morgenstern, XVIII ICPEAC Invited Papers, Aarhus, Denmark, p. 766, 1993.

⁸H. Winter, Europhys. Lett 18, 207 (1992); H. Winter, C. Auth, R. Schuch, and E. Beebe, Phys. Rev. Lett 71, 1939 (1993).

⁹S.T. de Zwart, T. Fried, U. Jellen, A.L. Boers, and A.G. Drentje, J. Phys. B18, L623 (1985).

¹⁰L. Folkerts and F.W. Meyer, Phys. Rev. A. to be submitted (1994).

¹¹B. Hird and F. Rahman, Phys. Rev. A26, 3108 (1982); B. Hird, F. Rahman, and M.W. Orakzai, Can. J. Phys. 66, 972 (1988).

¹²Niehof and W. Heiland, NIM B48, 306 (1990).

¹³L. Folkerts, S. Schippers, D.M. Zehner, and F.W. Meyer, submitted to Phys. Rev. Lett. 1994.

¹⁴e.g. H. Winter, Comments At. Mol. Phys. 26, 287 (1991).

¹⁵J. Burgdörfer, P. Lerner, and F.W. Meyer, Phys. Rev. A44, 5674 (1991).

Figure Captions

Fig. 1. Schematic side and top views of the collision geometry and experimental layout.

Fig. 2. Intensity distribution of scattered ions recorded on the PSD for (a.) 3.75 keV/amu O^{8+} ions incident at 1.8° , and (b.) for 2.0 keV/amu Ar^{11+} ions incident at 1.5° , both along the [110] direction of Au(110), illustrating the banana-shaped angular scattering distribution characteristic of surface-channeling.

Fig. 3. Intensity distribution recorded on the PSD with narrow slit opening and deflection voltage switched on, for 3.75 keV O^{8+} incident ions, showing charge states -1 (furthest on right) through +5 (furthest on left).

Fig. 4. Collapse of selected portions the 2D spectrum of Fig. 3 onto the (a.) vertical axis, showing the angular scattering distribution for four scattered charge states, and onto (b.) the horizontal axis showing the charge distribution of the scattered projectiles.

Fig. 5. Scattered projectile charge fractions for 3.75 keV/amu O^{q+} ($3 \leq q \leq 8$) ions incident along the [110] direction of Au(110) at 1.8° .

Fig. 6. Scattered projectile charge fractions for 1.2 keV/amu Ar^{q+} ($3 \leq q \leq 14$) ions incident along the [001] direction of Au(110).

Fig. 7. O^- scattered charge fractions for O^{1+} , O^{5+} , O^{7+} incident ions as a function of parallel velocity; incidence angle 1.8° along the [001] direction of Au(110); inset schematically indicates O^- formation mechanism.

Fig. 8. Simulated scattered projectile intensity distribution on the PSD for 3.75 keV/amu oxygen ions incident along the [110] direction of Au(110) at 1.8° , showing the characteristic banana-shaped angular scattering distribution observed for surface-channeling.

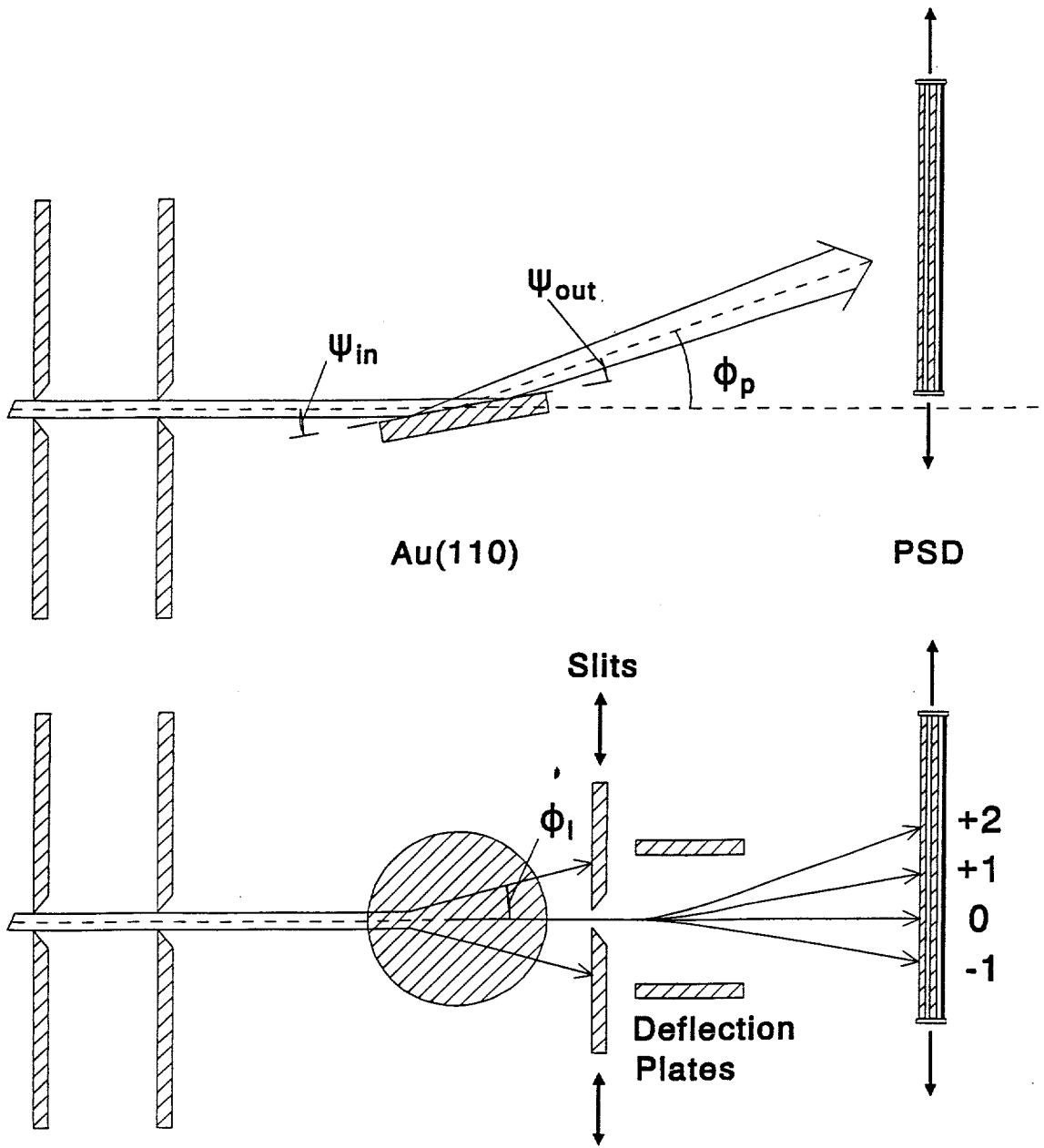
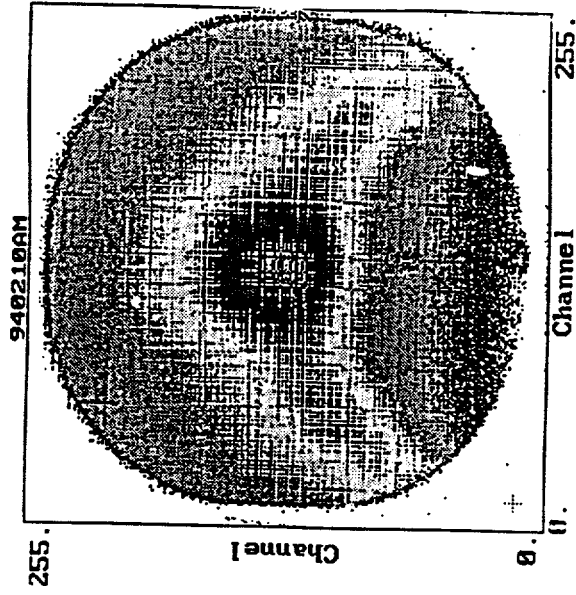
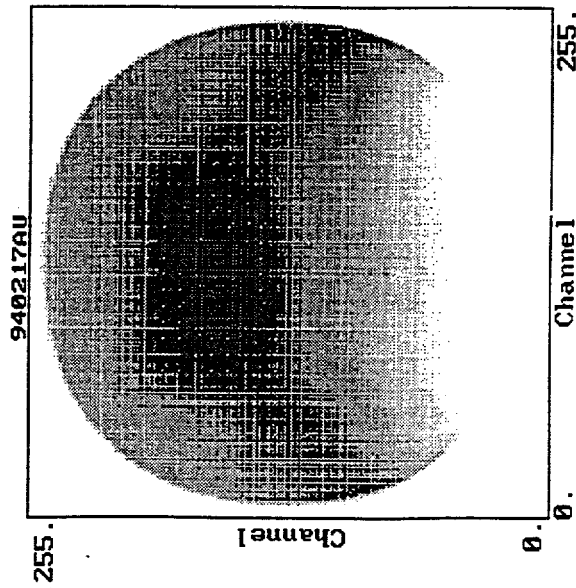


Fig. 1

Counts:
 1000.
 610.5
 372.8
 227.6
 138.9
 84.83
 51.79
 31.62
 19.31
 11.79
 7.197
 4.394
 2.683
 1.638
 1.000



b.)



a.)

Fig. 2

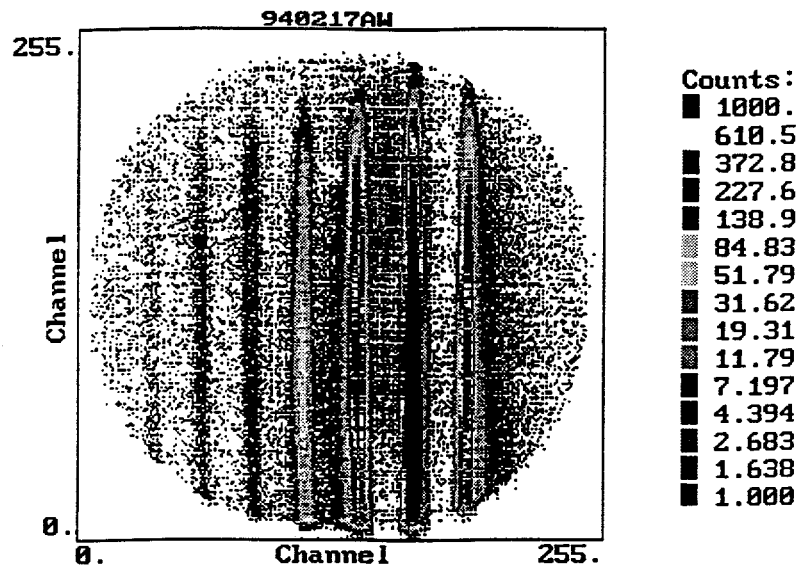
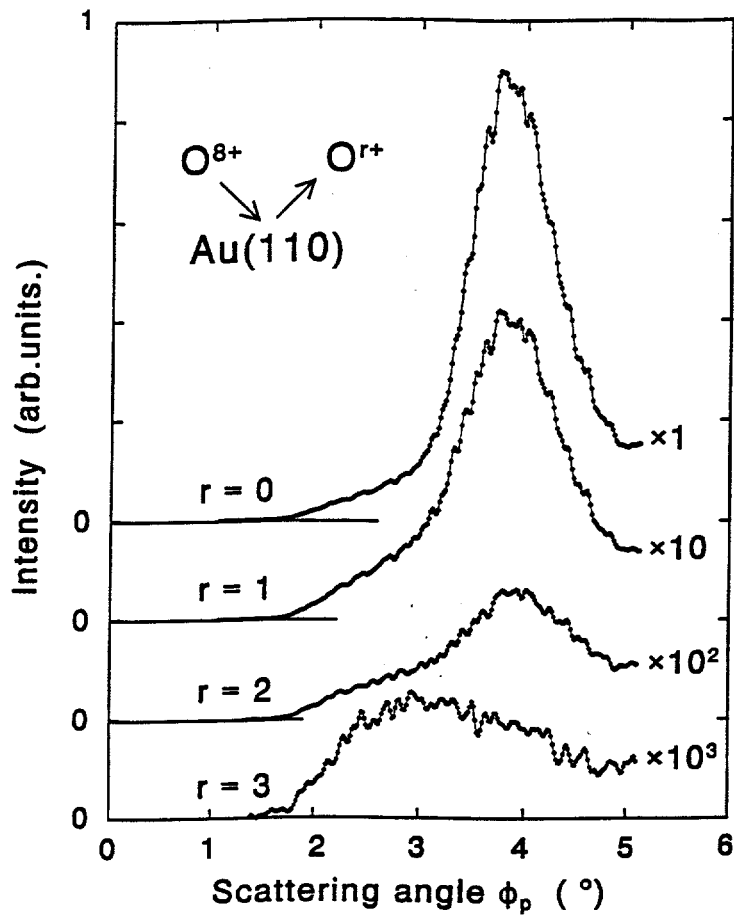
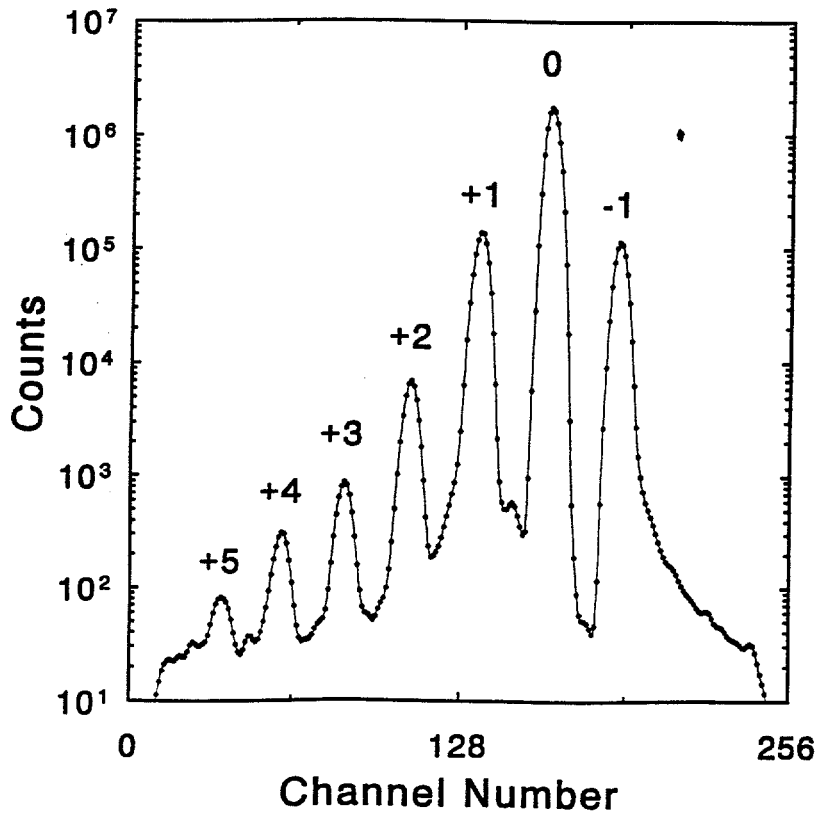


Fig. 3



a.)



b.)

Fig. 4

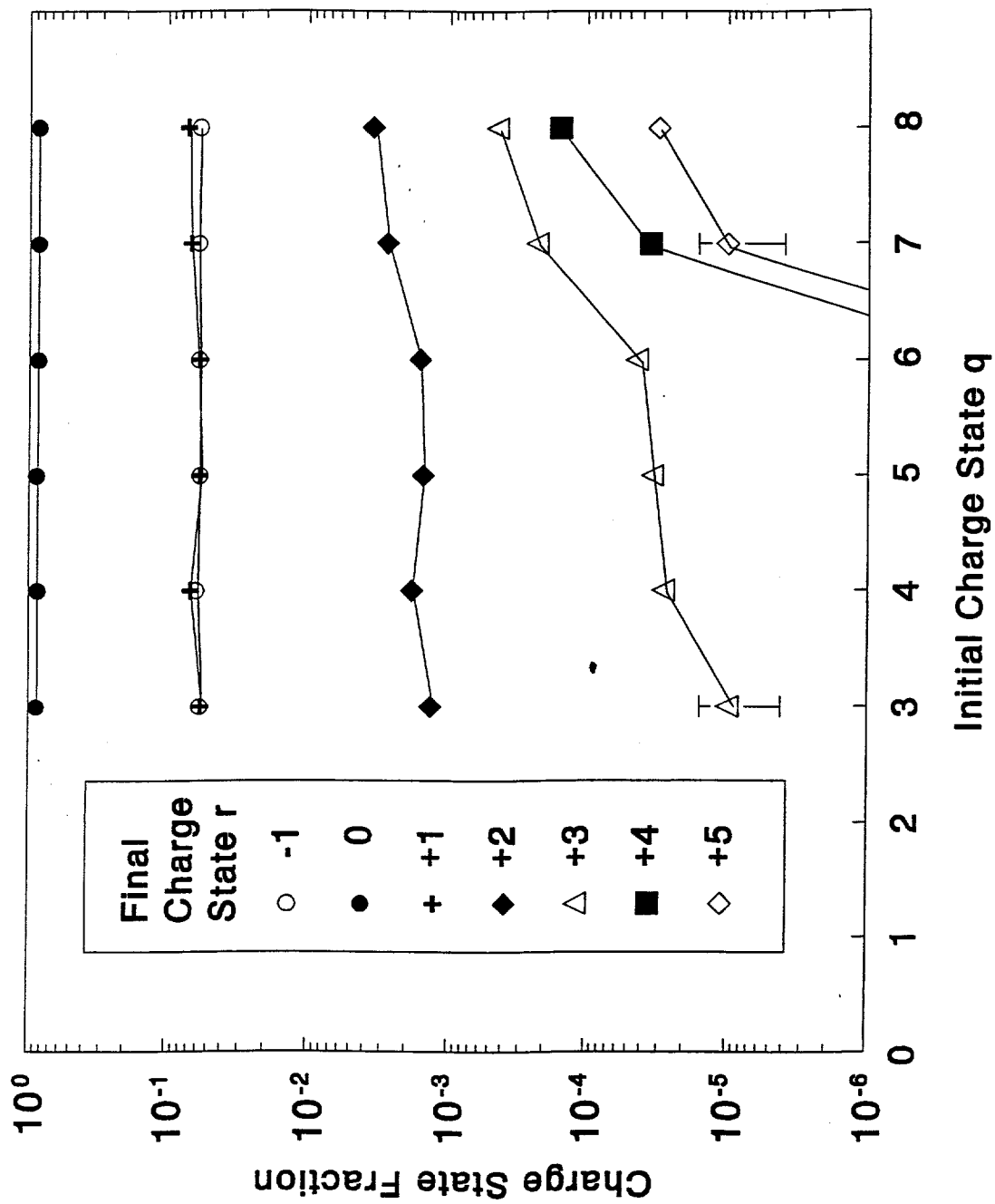


Fig. 5

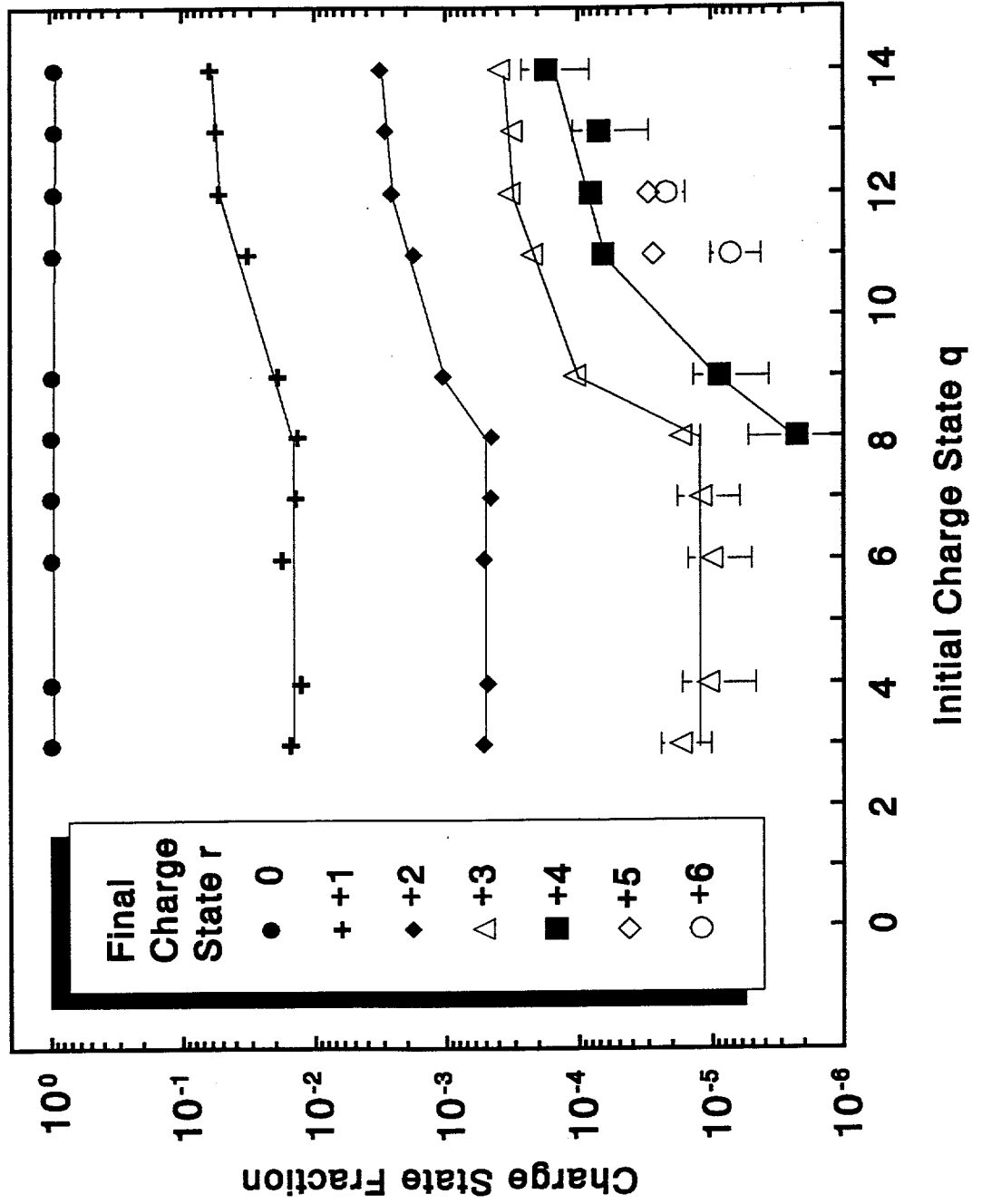


Fig. 6

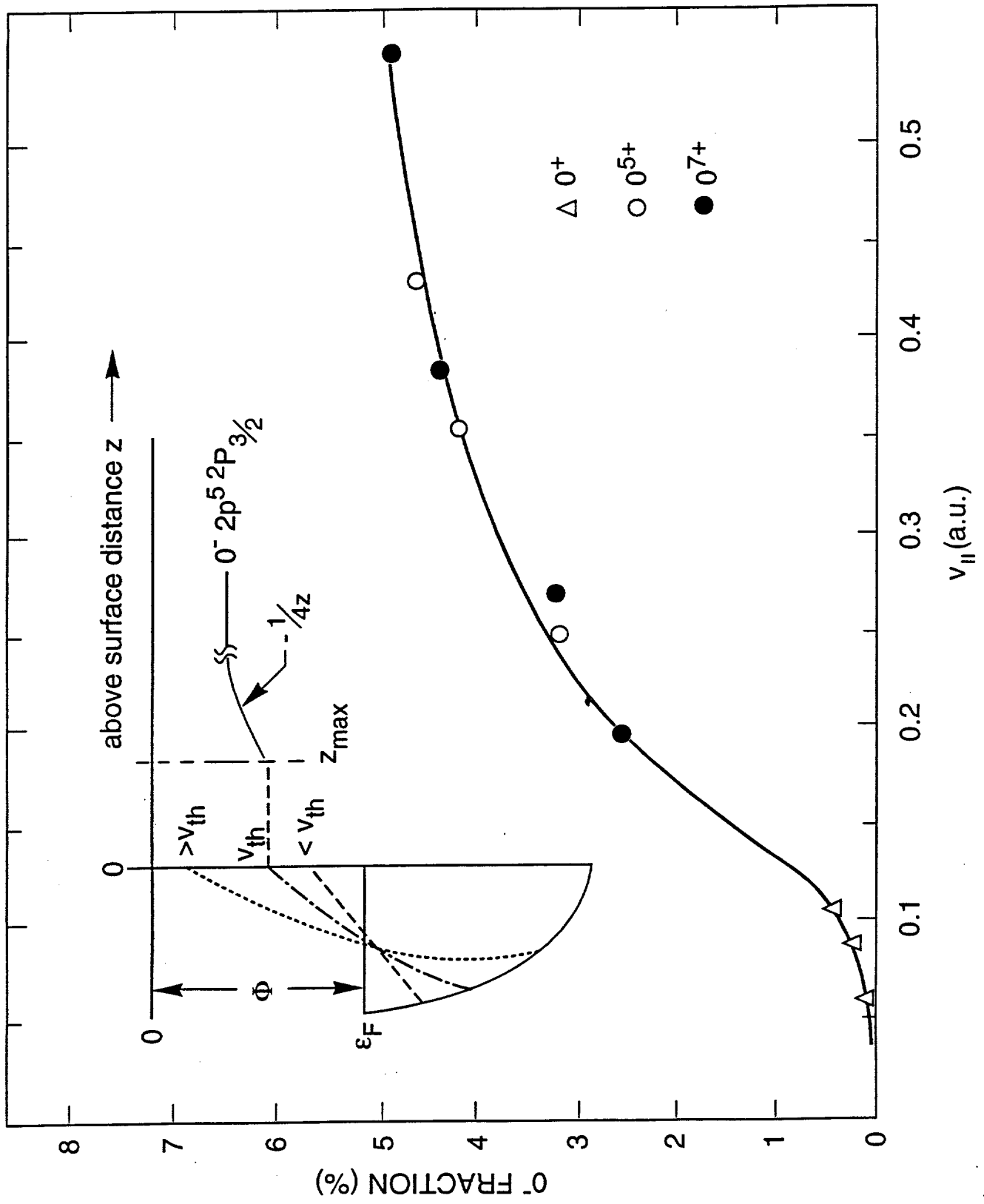


Fig. 7

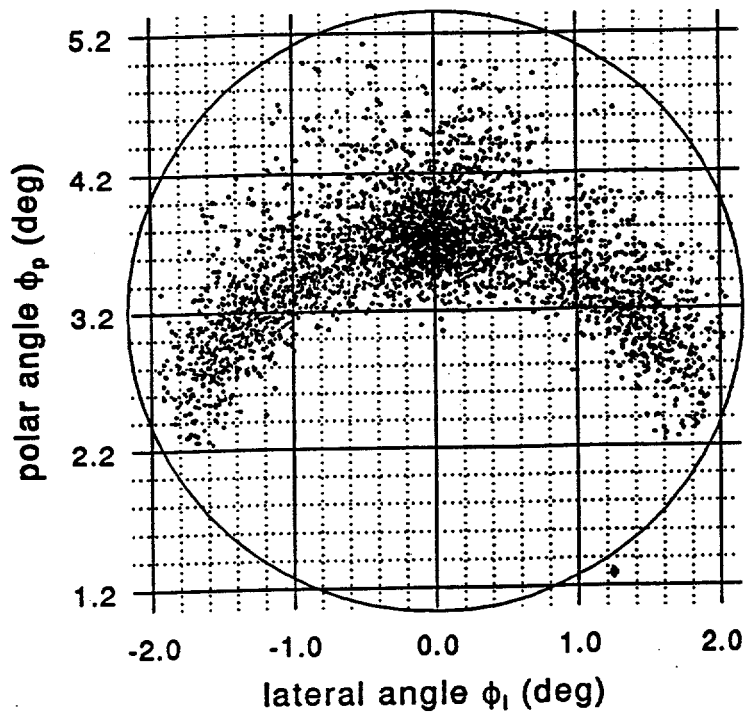


Fig. 8